PDE-BASED MODELING, CONTROL, AND STABILITY ANALYSIS OF HETEROGENEOUS THERMOSTATICALLY CONTROLLED LOAD POPULATIONS

Azad Ghaffari
Department of MAE
UC San Diego
La Jolla, CA 92039-0411
Email: aghaffari@ucsd.edu

Scott Moura
Department of Civil and Environmental Engineering
UC Berkeley
Berkeley, CA 94720
Email: smoura@berkeley.edu

Miroslav Krstić
Department of MAE
UC San Diego
La Jolla, CA 92039-0411
Email: krstic@ucsd.edu

ABSTRACT

Thermostatically controlled loads (TCLs) account for more than one-third of U.S. electricity consumption. Various techniques have been used to model TCL populations. A high-fidelity analytical model of Heterogeneous TCL (HrTCL) populations is of special interest for both utility managers and customers (that facilitates the aggregate synthesis of power control in power networks). We present a deterministic hybrid partial differential equation (PDE) model which accounts for HrTCL populations, and facilitates analysis of common scenarios like cold load pick up, cycling, and daily and/or seasonal temperature changes to estimate the aggregate performance of the system. The proposed technique is flexible in terms of parameter selection and ease of changing the set-point temperature and deadband width all over the TCL units. We investigate the stability of the proposed model along with presenting guidelines to maintain the numerical stability of the discretized model during computer simulations. Moreover, the proposed model is a close fit to design feedback algorithms for power control purposes. Hence, we present output and state feedback control algorithms, designed using the comparison principle and Lyapunov analysis, respectively. We conduct various simulations to verify the effectiveness of the proposed modeling and control techniques.

1 Introduction

In this paper we present, for the first time, an analytical model for heterogeneous thermostatically controlled load (TCL) populations. Also, we provide rigorous analysis to verify stability and accuracy of the proposed model. We design and investigate output feedback and state feedback for reference power tracking objectives. This work follows the long line of analytical and numerical modeling of TCL populations including heating, ventilation, and air conditioning (HVAC) systems, particularly for demand response studies in power networks [1–14].

One can refer to [12, 14] among the very first reports that used statistical and stochastic analysis to develop an aggregate model of TCLs. The effect of capital stock, lifestyle, usage response, and price impacts on power curves have been studied in [5,13]. Reference [11] presents a brief survey on five different TCL modeling techniques developed up to 1990. More recently, TCL modeling has gained extensive attention [1–4,6–10,15,16].

Coupled Fockker-Planck equations (CFPE), derived in [12], present statistical aggregate electrical dynamics for a homogeneous group of devices. A perturbation analysis yields the dynamics for a non-homogeneous group. Equations (10)–(18) of [12] include CFPE, 4 algebraic boundary conditions, and 2 ordinary differential equations to guarantee probability conservation. Moreover, the expectation of the operating state of the homogeneous population is given by another ODE defined by (43) in [12]. The proposed model does not provide direct access to manipulate the deadband and set-point temperature which makes the controller design process a hard task to achieve. An exact solution to the CFPE which describes the aggregate behavior of TCL populations is presented in [8]. Also, [8] demonstrates the potential to provide ancillary services by remotely manipulating thermostat set-points, particularly to balance fluctuations from intermittent renewable generators.

Another statistical model based on the "state bin transition model" has been developed in [10], a formal abstraction of which is presented in [9] to relax some of the assumptions in [10].

These statistical models rely on probability analysis and distribution functions to predict TCL population evolution.

A simpler deterministic model with ability to manipulate the set-point temperature using the sliding mode control (SMC) has been presented in [1] which eliminates the difficulties associated with statistical modeling and control techniques. The authors propose 2 averaged transport PDEs coupled on the deadband boundaries to model the population of on and off units. Using finite differentiation, the authors present bilinear dynamics for the purpose of power control. The model of [1] does not account for the effect of heterogeneity in TCL populations.

Reference [2] uses diffusion-advection PDEs to simulate the damping effect of heterogeneous populations in the power consumption curve. Also, the latter paper presents a distributed identification technique to estimate the parameters of the diffusion-advection PDEs. The diffusion-advection model of [2] is developed based on a phenomenological observation and it requires tuning the diffusion coefficient. On the contrary, our proposed analytical model captures the TCL population power dynamics using the system's physical characteristics and requires no tuning.

We highlight our objectives as follows: i) We develop analytical deterministic PDE dynamics for HrTCL populations which precisely simulate power changes under environment temperature fluctuations. Each group of homogeneous TCL units share 4 transport PDEs coupled through 4 algebraic boundary conditions on 4 different temperature levels. ii) We investigate the stability of the proposed model along with presenting guidelines to guarantee the numerical stability of the discretized dynamics. iii) We design output and state feedback control algorithms such that the system tracks a defined power curve regardless of environmental temperature variation. We actuate the set-point temperature which is a common input for all the TCLs. Because of its ability to estimate the power consumption dynamics, the proposed model could be augmented into load management programs. Also, one can use the proposed model to study power control via price incentives or to analyze the impact of various demand response policies.

The rest of this paper is organized as follows: Section 2 presents the model development. We discuss model stability in Section 3 . Model discretization and its numerical stability for simulation purposes along with model verification are presented in Section 4. Section 5 describes the output and state feedback design and provides stability analysis of the power control loop. The simulation results are given in Section 6. Section 7 concludes the paper.

2 Aggregate PDE-based Model

The operating state of an individual TCL is controlled by a thermostat whose state depends on temperature. It can be modeled as a hybrid system including one continuous state, temperature, and a discrete state, operating status e.g. cooling or heating, as introduced in [14].

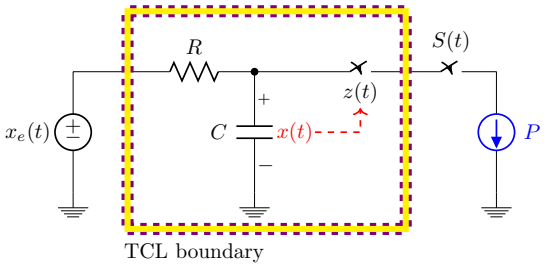

Figure 1. Equivalent electrical circuit of a TCL unit.

We consider the heterogeneity effect by dividing the TCL population into m homogeneous TCL groups. Assume that the temperature of TCL unit j in group i and environmental temperature are x_{ij} and x_e, respectively. As shown in Fig. 1, each TCL unit is modeled as a thermal capacitance, C_i kWh/°C, in series with a thermal resistance, R_i °C/kW, for $i = 1,2,\cdots,m$. All physical parameters are considered as constant values in each homogeneous group. The discrete state z_{ij}, modeled by a Schmitt trigger switch shown in Fig. 2, denotes whether the load is on or off. The power injected to each unit in TCL group i equals P_i kW.

The hybrid dynamics of unit j in TCL group i for a cooling system are defined as follows

$$\frac{\mathrm{d}x_{ij}(t)}{\mathrm{d}t} = \frac{x_e(t) - x_{ij}(t) - z_{ij}(t)S_i(t)R_iP_i}{R_iC_i} \tag{1}$$

$$z_{ij}(t) = \begin{cases} 1 & x_{ij}(t-\mathrm{d}t) \geq x_H \\ z_{ij}(t-\mathrm{d}t) & x_L < x_{ij}(t-\mathrm{d}t) < x_H \\ 0 & x_{ij}(t-\mathrm{d}t) \leq x_L \end{cases}, \tag{2}$$

for $i = 1,2,\cdots,m$ and $j = 1,2,\cdots,n_i$, where $x_L = x_{\mathrm{sp}} - \sigma$ and $x_H = x_{\mathrm{sp}} + \sigma$, where x_{sp} is the set-point temperature and 2σ is the deadband width. A proper combination of temperature resistance and cooling power ensures temperature drop during on

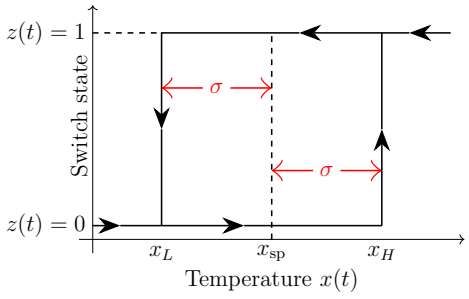

Figure 2. Characteristic of the switch modeled as a Schmitt trigger.

state. This necessary condition is given as

$$x_e(t) - x_{ij}(t) < R_i P_i, \tag{3}$$

and will be used in model stability analysis. We assume the entire TCL population share the same x_{sp} and σ. The utility manager has the ability to override a group's control system by turning off the supply switch, $S_i(t) = 0$. We assume that $S_i(t)$ is normally closed, $S_i(t) = 1$. The aggregate power is given by

$$y(t) = \sum_{i=1}^{m} \left(\frac{P_i}{\eta_i} S_i(t) \sum_{j=1}^{n_i} z_{ij}(t) \right), \tag{4}$$

where η_i is the performance coefficient for TCL group i.

We assume uniform environmental temperature, x_e, for all TCL units. We assume $x \in [x_{\min}, x_{\max}]$, where the lowest and highest feasible temperature is given by $x_{\min}$ and $x_{\max}$, respectively. As shown in Fig. 3, we select a homogeneous population of TCLs that have identical hybrid dynamics (1) and (2) and are subject to the same control within a load management program, the same $S_i(t)$ [12]. The density of the TCL units per temperature is a distribution over i. This distribution is given by $\mu_{i,kl}(t,x)$ for TCL group i. Subscript k denotes if TCLs are on ($k = 1$) or off ($k = 0$). Subscript l denotes the temperature region a, b, and c corresponding to $x \in (x_H, x_{\max})$, $x \in (x_L, x_H)$, and $x \in (x_{\min}, x_L)$, respectively.

Since we develop our model for arbitrary homogeneous TCL group i, from this point forward we drop subscript i from the distribution function. However, one should keep in mind all states are 1-D temporal and 2-D spatial (x, i). In each homogeneous group, the TCL flux which indicates the number of TCLs passing a certain temperature per second is obtained as follows

$$\varphi(t,x) = \mu(t,x) \frac{\Delta x}{\Delta t}. \tag{5}$$

Taking the limit of the above equation when $\Delta t \to 0$ and using

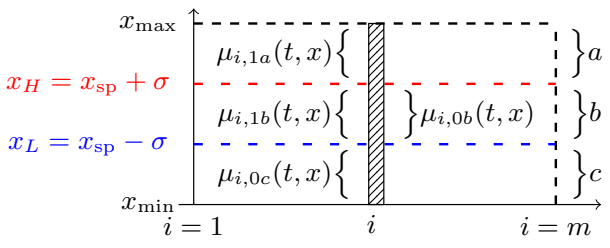

Figure 3. Distribution functions of TCLs in three regions.

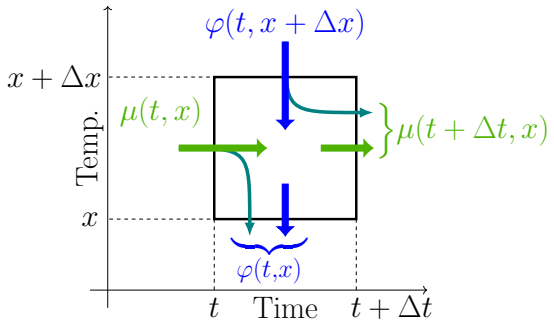

Figure 4. Population variation of on units over an infinitesimal time-temperature window. The graph is presented for a homogeneous population.

(1) gives

$$\varphi(t,x) = \mu(t,x) \frac{x_e(t) - x - zSRP}{RC}, \tag{6}$$

which indicates the relationship between time and temperature density of TCL units. We are interested in finding a time-temperature differential equation which describes the evolution of $\mu(t,x)$ over time at a certain temperature level. Hence, we present Fig. 4 to obtain the relationship between variation of TCL population flux, $\varphi(t,x)$, with respect to temperature and variation of TCL population distribution, $\mu(t,x)$, with respect to time.

In order to understand Fig. 4, we assume two extreme cases. First, TCL's time constant, RC, is considerably large such that temperature variation of a TCL unit is negligible. Hence, temperature of TCL units evolve with zero slope which means flux variation is zero. Second, the time constant is considerably small. Under this condition, temperature of each TCL unit evolves with infinite slope which means all units instantly change place between x_L and x_H. This means $\mu(t,x)$ does not change over time.

When RC changes in a moderate fashion, we have a combination of both features. TCL population distribution is time-varying, introduced by $\mu(t,x)$. TCL population flux, $\varphi(t,x)$, indicates the number of TCL units passing through a certain temperature at a given time. Energy is conserved over TCL populations. Moreover, TCLs do not appear or disappear inside a time-temperature window without passing the window boundaries. Thus, the total rate of variation of TCLs in a time-temperature window is zero

$$\frac{\mu(t+\Delta t,x) - \mu(t,x)}{\Delta t} + \frac{\varphi(t,x+\Delta x) - \varphi(t,x)}{\Delta x} = 0. \tag{7}$$

Taking the limit of the above equation when $\Delta t \to 0$ and $\Delta x \to 0$

and using (6) we obtain

$$\frac{\partial \mu(t,x)}{\partial t} = -\frac{\partial}{\partial x}\left(\mu(t,x)\frac{x_e - x - zSRP}{RC}\right), \tag{8}$$

which defines the system dynamics of the TCLs in all regions of Fig. 3

$$\frac{\partial \mu_{kl}(t,x)}{\partial t} = -\frac{\partial}{\partial x}\left(\mu_{kl}(t,x)\frac{x_e - x - kSRP}{RC}\right), \tag{9}$$

where $kl = 0c, 0b, 1b, 1a$. We need 4 boundary conditions to solve the dynamics equations of (9). The flux is conserved at x_H and x_L

$$\varphi_{0b}(t,x_H) + \varphi_{1b}(t,x_H) = \varphi_{1a}(t,x_H) \tag{10}$$
$$\varphi_{0b}(t,x_L) + \varphi_{1b}(t,x_L) = \varphi_{0c}(t,x_L), \tag{11}$$

then using (6) we obtain

$$\mu_{1b}(t,x_H) = \mu_{1a}(t,x_H) + \lambda_0 \mu_{0b}(t,x_H) \tag{12}$$
$$\mu_{0b}(t,x_L) = \mu_{0c}(t,x_L) + \lambda_1 \mu_{1b}(t,x_L), \tag{13}$$

for all $t \in [0,\infty)$, where

$$\lambda_0 = -\frac{x_e - x_H}{x_e - x_H - RP} > 0 \tag{14}$$
$$\lambda_1 = -\frac{x_e - x_L - RP}{x_e - x_L} > 0. \tag{15}$$

Temperatures higher than $x_{\max}$ are shown by $x^+_{\max}$. Temperatures lower than $x_{\min}$ are shown by $x^-_{\min}$. Since there is no unit higher than $x_{\max}$ or lower than $x_{\min}$, the following conditions are valid

$$\mu_{1a}(x^+_{\max}) = 0 \tag{16}$$
$$\mu_{0c}(x^-_{\min}) = 0, \tag{17}$$

for all $t \in [0,\infty)$. The system of (9) along with (12), (13), (16), and (17) define the evolution of TCLs over time and temperature for every $i = 1, 2, \cdots, m$. The number of on units per i equals

$$\rho_i(t) = \int_{x_L}^{x_H} \mu_{i,1b}(t,x)\mathrm{d}x + \int_{x_H}^{x_{\max}} \mu_{i,1a}(t,x)\mathrm{d}x, \tag{18}$$

where $i = 1, 2, \cdots, m$ and the power consumption for the entire TCL population is calculated as

$$y(t) = \sum_{i=1}^{m} \frac{P_i}{\eta_i}\rho_i(t). \tag{19}$$

3 Model Stability

In an operating cooling system, after transient is passed, there are no TCL units in regions a and c. All TCL units are in region b in either on or off state and system dynamics are given as

$$\frac{\partial \mu_{1b}}{\partial t} = -\left(\frac{x_e(t) - x - RP}{RC}\right)\frac{\partial \mu_{1b}}{\partial x} + \left(\frac{1}{RC}\right)\mu_{1b} \tag{20}$$
$$\frac{\partial \mu_{0b}}{\partial t} = -\left(\frac{x_e(t) - x}{RC}\right)\frac{\partial \mu_{0b}}{\partial x} + \left(\frac{1}{RC}\right)\mu_{0b}, \tag{21}$$

with the following boundary conditions

$$\mu_{1b}(x_H) = \lambda_0 \mu_{0b}(x_H) \tag{22}$$
$$\mu_{0b}(x_L) = \lambda_1 \mu_{1b}(x_L). \tag{23}$$

Transport PDEs of (20) and (21) have the same reaction term with constant coefficient $1/RC$. The advection coefficient in both equations is time-varying with positive value in (20) and negative value in (21).

The total population of TCL units is given as

$$W(t) = \int_{x_L}^{x_H} \Big(\mu_{1b}(t,x) + \mu_{0b}(t,x)\Big)\mathrm{d}x, \tag{24}$$

which is a positive definite function and its time derivative is zero. This observation guarantees unvarying population which also means the system has a pole at the origin. The proposed population function, $W(t)$, and its time derivative do not provide further details on the system dynamics. Assuming a constant environment temperature, x_e, we use Laplace transformation to solve the system of (20) and (21). The Laplace transformation of function $f(t)$ is given as

$$\mathcal{L}f(s) = \int_0^{\infty} \mathrm{e}^{-st} f(t)\mathrm{d}t, \tag{25}$$

where s is a complex number. Applying Laplace transformation to (20) and (21) gives

$$\frac{\partial}{\partial x}\mathcal{L}\mu_{1b}(s,x) = -\left(\frac{RCs - 1}{x_e - x - RP}\right)\mathcal{L}\mu_{1b}(s,x) \tag{26}$$
$$\frac{\partial}{\partial x}\mathcal{L}\mu_{0b}(s,x) = -\left(\frac{RCs - 1}{x_e - x}\right)\mathcal{L}\mu_{0b}(s,x). \tag{27}$$

Since x_e is assumed constant, we can solve (26) and (27) for x

$$\frac{\mathcal{L}\mu_{1b}(s,x_H)}{\mathcal{L}\mu_{1b}(s,x_L)} = \left(\frac{x_H - x_e + RP}{x_L - x_e + RP}\right)^{RCs-1} \tag{28}$$

$$\frac{\mathcal{L}\mu_{0b}(s,x_H)}{\mathcal{L}\mu_{0b}(s,x_L)}=\left(\frac{x_e-x_H}{x_e-x_L}\right)^{RCs-1}. \tag{29}$$

Using boundary conditions (22) and (23) in (28) gives

$$\frac{\mathcal{L}\mu_{0b}(s,x_H)}{\mathcal{L}\mu_{0b}(s,x_L)}=\left(\frac{x_e-x_L}{x_e-x_H}\right)\left(\frac{x_H-x_e+RP}{x_L-x_e+RP}\right)^{RCs}. \tag{30}$$

Recall

$$1=\mathrm{e}^{\pm 2k'\pi\mathbf{j}},\quad \mathbf{j}=\sqrt{-1},\quad k'=0,1,2,\cdots, \tag{31}$$

then from (29) and (30) we obtain

$$s=\pm k'\omega\mathbf{j}, \tag{32}$$

where

$$\omega=\frac{2\pi}{RC\ln\left(\frac{(x_e-x_L)(x_H-x_e+RP)}{(x_e-x_H)(x_L-x_e+RP)}\right)}, \tag{33}$$

which indicates the system response only happens at certain frequencies. System parameters and environment temperature, x_e, define the base frequency, ω. According to Fourier transformation, the time response is composed of infinite number of oscillators with central frequency of $k'\omega$. This indicates the TCL population has one pole at the origin and infinite number of conjugate poles on imaginary axis. The results of this section is presented in the following statement.

Remark 1. *System dynamics of* (20) *and* (21) *with boundary conditions of* (22) *and* (23) *guarantee unvarying TCL population. Moreover, the system poles are distributed on the imaginary axis as given by* (32).

4 Finite Difference and Numerical Verification

In Section 3 we investigated model stability in continuous time and space. However, for numerical simulation the equations need to be discretized. Recall that the units in regions a and c eventually enter the deadband and the system dynamics are given by (20) and (21) with boundary conditions of (22) and (23). Regardless of the selected discretization method uncoupled discretized versions of (20) and (21) remain stable. Variation of TCL population caused by population rollover on the boundaries, defined by (22) and (23), can destabilize the system. Hence, the boundary conditions (22) and (23) need to be modified to ensure stability after system discretization.

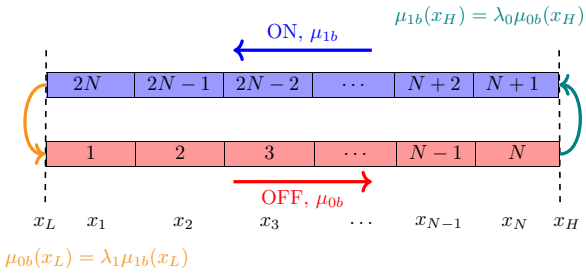

Figure 5. The method of finite difference applied for discretization of the transport PDEs to use in numerical simulations.

We suggest the forward and backward finite difference methods for on and off units, respectively. However, care has to be taken that the population of the TCL units remains unchanged during the numerical simulation. This property is achieved by maintaining one pole at zero as described in Remark 1. As shown in Fig. 5, we divide the deadband region into N equal temperature bins, Δx. By applying the method of finite difference to (20) and (21) we get

$$\frac{\mathrm{d}\mu_i}{\mathrm{d}t}=(\alpha-\alpha_i)\mu_i+\alpha_i\mu_{i-1} \tag{34}$$

$$\frac{\mathrm{d}\mu_{N+i}}{\mathrm{d}t}=(\alpha-\alpha_{N+i})\mu_{N+i}+\alpha_{N+i}\mu_{N+i-1}, \tag{35}$$

where $i=2,3,\cdots,N$, $\mu_1=\lambda_1\mu_{2N}$, $\mu_{N+1}=\lambda_0\mu_N$, $\alpha=1/(RC)$, and

$$\alpha_i=\frac{(x_e-x_i)}{RC\Delta x}>0 \tag{36}$$

$$\alpha_{N+i}=\frac{RP-(x_e-x_{N+1-i})}{RC\Delta x}>0, \tag{37}$$

where $i=2,3,\cdots,N$. Trivially $\alpha_i>0$ and from (3) we know $\alpha_{N+i}>0$. Since Δx is enough small in comparison to x_e-x_i and $RP-(x_e-x_{N+1-i})$, then $\alpha_i-\alpha>0$ and $\alpha_{N+i}-\alpha>0$. The characteristic equation of the system dynamics equals

$$G(s)=\prod_{\substack{i=2\\ i\neq N+1}}^{2N}(s+\alpha_i-\alpha)-\lambda_0\lambda_1\prod_{\substack{i=2\\ i\neq N+1}}^{2N}\alpha_i=0. \tag{38}$$

Occurrence of one eigenvalue at zero is guaranteed if λ_0 and λ_1 are redefined as follows

$$\lambda_0'=\kappa\lambda_0 \tag{39}$$

$$\lambda_1'=\kappa\lambda_1, \tag{40}$$

where

$$\kappa = \prod_{\substack{i=2 \\ i\neq N+1}}^{2N} \sqrt{\frac{\alpha_i - \alpha}{\alpha_i \lambda_0 \lambda_1}}. \tag{41}$$

Remark 2. *One requires the discretized model to retain a "conservation of matter" property, meaning that the TCLs don't disappear or appear over time. This mathematically means the discretized equations should have a pole at the origin. Since the TCL population is not changing, when numerical simulations based on the finite difference method are conducted, the boundary conditions of* (20) *and* (21) *need to be corrected by replacing* (22) *and* (23) *with* (39) *and* (40)*, respectively. The corrector* κ *defined by* (41) *guarantees that a pole happens at zero at each time step and the TCL population remains unchanged during the course of simulation.*

We present the approximate location of the other poles of the corrected discretized equation in order to show the stability of the discretized system dynamics. A low number of temperature bins does not generate a precise model to reconstruct the system characteristics. Our numerical analysis shows that for $N < 4$ the discretized equations do no catch the system dynamics.

Assume $N = 4$, then the system characteristic equation of (38) after using (39) and (40) and neglecting α gives

$$\begin{aligned} G(s) = & s^6 + 3\beta_1 s^5 + \Big(3\beta_1^2 + \beta_2 + \beta_3 + \beta_4\Big)s^4 + \\ & + \Big(\beta_1^3 + 2\beta_1(\beta_2 + \beta_3 + \beta_4)\Big)s^3 + \\ & + \Big(\beta_1^2(\beta_2 + \beta_3 + \beta_4) + \beta_2\beta_3 + \beta_2\beta_4 + \beta_3\beta_4\Big)s^2 \\ & + \beta_1\Big(\beta_2\beta_3 + \beta_2\beta_4 + \beta_3\beta_4\Big)s, \end{aligned} \tag{42}$$

where

$$\beta_1 = \frac{P}{C\Delta x} \tag{43}$$

$$\beta_i = \alpha_i(\beta_1 - \alpha_i) > 0, \quad i = 2,3,4. \tag{44}$$

We rewrite (42) as follows

$$G(s) = s(s+\beta_1)\hat{G}(s), \tag{45}$$

where

$$\begin{aligned} \hat{G}(s) = & s^4 + 2\beta_1 s^3 + \Big(\beta_1^2 + \beta_2 + \beta_3 + \beta_4\Big)s^2 + \\ & + \beta_1\Big(\beta_2 + \beta_3 + \beta_4\Big)s + \beta_2\beta_3 + \beta_2\beta_4 + \beta_3\beta_4, \end{aligned} \tag{46}$$

which indicates one pole at zero and another pole at $-\beta_1$ which its place on the real axis is inversely related to the temperature bin width, Δx. Assume

$$\beta_2 + \beta_3 + \beta_4 = \frac{\beta_1^2}{2}(1 - \cos\psi) \tag{47}$$

$$\beta_2\beta_3 + \beta_2\beta_4 + \beta_3\beta_4 = \frac{\beta_1^4}{8}(1 - \cos\psi), \tag{48}$$

which gives

$$\hat{G}(s) = \prod_{n=1}^{4}\left(s + \frac{\beta_1}{2}\Big(1 + \exp(\mathbf{j}\phi_n)\Big)\right), \tag{49}$$

where

$$\phi_n \in \left\{\frac{\psi}{2}, \pi - \frac{\psi}{2}, \pi + \frac{\psi}{2}, 2\pi - \frac{\psi}{2}\right\}, \quad n = 1,2,3,4. \tag{50}$$

Since σ is very small in comparison to x_e and x_{sp}, we can approximate $\alpha_2 = \alpha_3 = \alpha_4$, then an estimate of ψ using (47) and (48) is obtained

$$\psi = \frac{2\pi}{3}. \tag{51}$$

The other solution, $\psi = 0$, is affiliated with $s = 0$ and $s = -\beta_1$. For $N \geq 4$, where N is an even number, the system poles are approximated as

$$p_i \in \left\{0, -\frac{\beta_1}{2}\Big(1 + \exp(\mathbf{j}\phi)\Big), -\beta_1\right\}, i = 1,2,\cdots,2N-2, \tag{52}$$

where

$$\phi = \pm k'\left(\frac{\pi}{N-1}\right), \quad k' = 1,2,\cdots,N-2, \tag{53}$$

which defines a circle with center of $(-\beta_1/2, 0)$ and radius of $-\beta_1/2$. This result is in keeping with Remark 1. Reducing Δx toward zero pushes the pole locus radius toward infinity and ultimately the imaginary axis will become a part of the pole locus with the origin a part of the locus.

Applying the method of finite difference to the TCL dynamics of (20) and (21), when all the TCL units are located inside the

deadband, creates the linear state space of (34) and (35) which can be written in matrix form

$$\frac{d\xi}{dt} = A\xi, \quad A \in \mathbb{R}^{2N-2} \times \mathbb{R}^{2N-2}, \tag{54}$$

where

$$\xi = \left[\mu_2,\ \mu_3,\ \cdots,\ \mu_N,\ \mu_{N+2},\ \mu_{N+3},\ \cdots,\ \mu_{2N}\right]^T. \tag{55}$$

Discretizing (54) with the time step of Δt generates

$$\xi_n = \hat{A}\xi_{n-1}, \quad \hat{A} = (I_{(2N-2)\times(2N-2)} + A\Delta t), \tag{56}$$

and the eigenvalues of $\hat{A}$ vary between one and $1-\beta_1\Delta t$. The system of (56) is stable for

$$1 - \beta_1 \Delta t \geq -1. \tag{57}$$

Also, recall that $N = 2\sigma/\Delta x$ and $N \geq 4$, hence

$$\frac{P}{2C}\Delta t \leq \Delta x \leq \frac{\sigma}{2}, \tag{58}$$

which indicates the relationship between the time and temperature steps to guarantee stability of (56). The time constant of the TCL population satisfies $RC \geq L_\tau$ where L_τ is a positive finite number. The time step needs to be considerably smaller than the least time constant, $\Delta t \ll L_\tau$.

Remark 3. *Equations* (34) *and* (35) *represent space discretization of the system dynamics of* (20) *and* (21) *where the temperature bin width is* $\Delta x = 2\sigma/N$. *We approximate the location of the system poles as* (52) *for an even number of temperature bins,* $N = 2k \geq 4$, *where* $k = 2,3,\cdots$, *which indicates that all the system poles are distributed evenly on a circle in the complex plane with the center of* $(-\beta_1/2, 0)$ *and radius of* $\beta_1/2$. *The angular distribution is defined by* (53). *Regardless of variation in system physical parameters as long as* Δx *is the same, the normalized pole locus remains the same. Furthermore, when time discretization is applied, if* (58) *is satisfied then the system dynamics remain stable.*

We compare our aggregate PDE-based model (9) against a Monte Carlo (MC) model generated from (1) and (2) . TCL units are initially distributed evenly between on and off units in the deadband in 10 groups, $m = 10$. The characteristic parameters are defined as $R_i = R_0 f(i), C_i = C_0 f(i), P_i = P_0/f(i)$, and $\eta_i = \eta_0/f(i)$, where $R_0 = 2\,^\circ$C/kW, $C_0 = 1$ kWh/°C, $P_0 = 10$ kW,

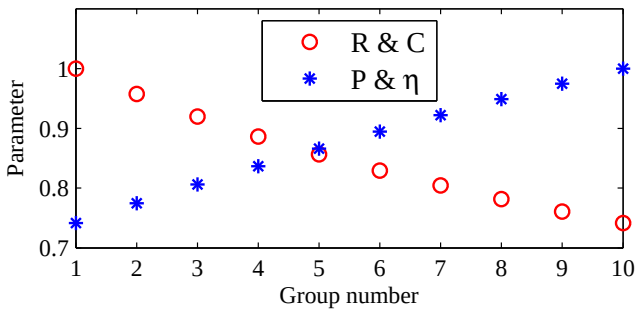

Figure 6. Normalized physical parameters.

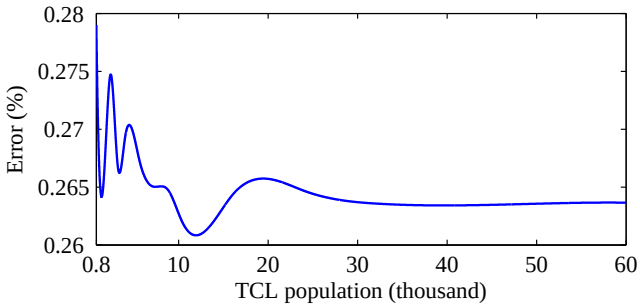

Figure 7. Variation of error between PDE and MC model versus TCL population.

$\eta_0 = 2.5$, and $f(i) = \sqrt{20/(10+i)}$ for $i = 1,2,\cdots,10$. The normalized parameters are shown in Fig. 6. Temperature values are given as $x_{sp} = 24\,^\circ$C, $\sigma = 1\,^\circ$C, $x_e = 35\,^\circ$C. For parameter selection see [11,13]. Since smaller RC means fast power dissipation, we choose P_i varying in the opposite direction of R and C. Also, for simplicity, we chose the power efficiency to be the same all over the TCL groups and equal $P/\eta = 4$. We discussed the effect of time and temperature steps on stability of discretized dynamics. Trivially, smaller values for Δt and Δx which satisfy (58) increase precision of the discretized model. TCL population, also, plays an important role in model precision. Hence, we compare the performance of the PDE-based against the MC model for different TCL populations. Our comparison function is relative error in energy estimation from time 0 to time $t_f = 2$ hour defined as

$$error := \int_0^{t_f} \frac{|y_{\text{PDE}}(t) - y_{\text{MC}}(t)|}{y_{\text{MC}}(t)} dt. \tag{59}$$

As Fig. 7 shows the error remains considerably small even for low TCL population. Populations more than 10,000 TCLs show the same error. In the following simulations we assume 40,000 TCL units divided in 10 homogeneous groups.

We present our first group of simulations to verify our proposed model and the results of Remark 2 and 3. Figure 8 shows

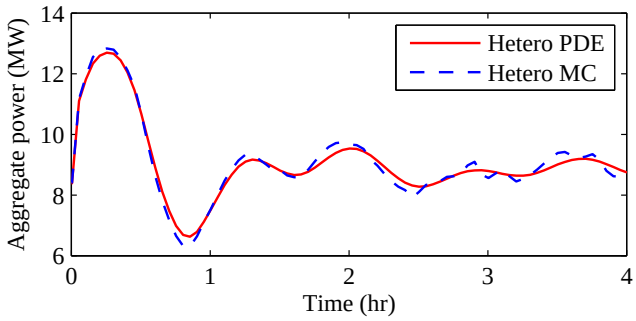

Figure 8. System response to a step change in the set-point temperature from 24.5 °C to 24 °C with $\sigma = 1$ °C for (solid red) our proposed PDE-based and (dashed blue) the MC model for 40,000 HrTCL units.

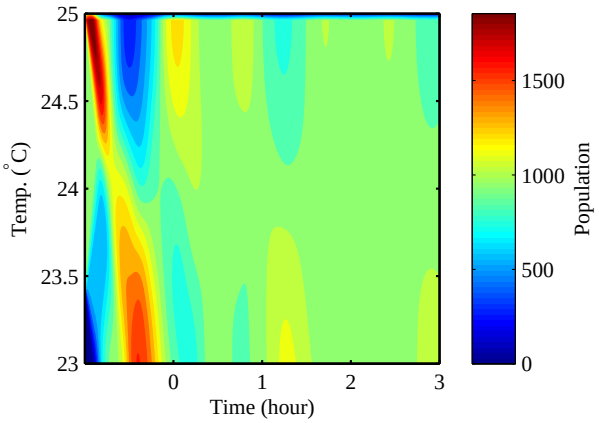

Figure 9. TCL population uniformly distributes after transient is passed.

the system response to a step change in the set-point temperature from 24.5 °C to 24 °C with $\sigma = 1$ °C. The proposed PDE-based model accurately captures the power dynamics of the HrTCL population. Figure 9 shows that after passing transient TCL units distribute uniformly from x_L to x_H. We remind the reader there is no TCL unit outside the deadband region. The normalized poles of the system under the proposed parameter distribution of Fig. 6 are evenly distributed on a unit circle as shown in Fig. 10.

In the next section we use the proposed model to design a reference tracking control to achieve power control in HrTCL populations.

5 Control Design and Stability Analysis

While the control actuators are distributed across the TCL units, a supervisory system can manipulate the set-point temperature and deadband width simultaneously to control the aggregate power consumption. The deadband width changes the power consumption curve to a lower extent. Sudden increases in power demand caused by dramatic fluctuation in environmental

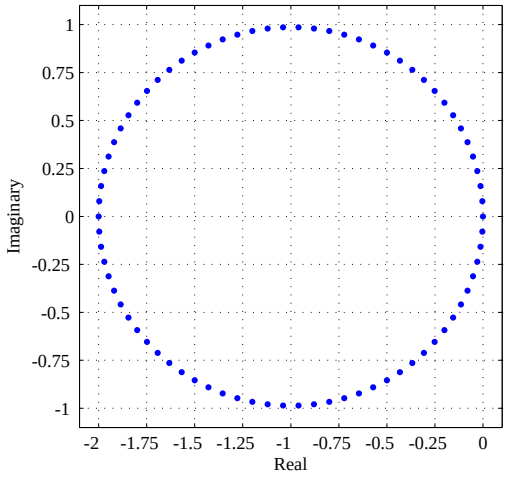

Figure 10. For a constant N, normalized pole locus remains the same regardless of parameter variation as shown in Fig. 6.

temperature or high transient peaks after power outage periods could potentially put the entire system at risk. Hence, the presence of a power control algorithm is necessary.

Various control algorithms for TCLs have been reported in the literature [1, 4, 8, 10]. Bashash and Fathy [1] reported aggregate power control using sliding mode control algorithm. Their proposed algorithm is based on simplified PDEs with averaged parameters for homogeneous TCL populations. Here, we show that a linear integral output feedback applied to the set-point temperature guarantees fast tracking of reference power provided that the integrator gain is selected properly. We design our control based on the coupled transport PDE model of (9), obtained for an arbitrary large number of HrTCLs, with the boundary conditions of (12), (13), (16), and (17).

Using (18) and denoting the flux equation of (6) on x_H and x_L boundaries, we can calculate the variation of the number of on units versus time as follows

$$\frac{d\rho}{dt} = \varphi_{0b}(x_H) + \varphi_{1b}(x_L) - \mu_{0b}(x_H)\dot{x}_H - \mu_{1b}(x_L)\dot{x}_L. \qquad (60)$$

The number of off units turning on equals $\varphi_{0b}(x_H)$ and the number of on units turning off equals $-\varphi_{1b}(x_L)$. The last 2 terms are added to consider the effect of time varying set-point temperature. Assume the switch deadband, σ, is fixed, and the rate of the set-point temperature is controlled by input u

$$\dot{x}_{sp} = u. \qquad (61)$$

We use (60) to calculate the time derivative of the consumed power (19)

$$\dot{y} = -c_1(t)u - c_2(t)x_{sp} + c_3(t)\sigma + c_4(t), \qquad (62)$$

where

$$c_1(t)=\sum_{i=0}^{m}\frac{P_i}{\eta_i}\Big(\mu_{i,1b}(t,x_L)+\mu_{i,0b}(t,x_H)\Big) \tag{63}$$

$$c_2(t)=\sum_{i=1}^{m}\frac{P_i}{\eta_i R_i C_i}\Big(\mu_{i,1b}(t,x_L)+\mu_{i,0b}(t,x_H,)\Big) \tag{64}$$

$$c_3(t)=\sum_{i=1}^{m}\frac{P_i}{\eta_i R_i C_i}\Big(\mu_{i,1b}(t,x_L)-\mu_{i,0b}(t,x_H)\Big)\leq c_2(t) \tag{65}$$

$$\begin{aligned}c_4(t)=&\sum_{i=1}^{m}\frac{P_i}{\eta_i R_i C_i}\Big((x_e(t)-R_iP_i)\mu_{i,1b}(t,x_L)+\\&+x_e(t)\mu_{i,0b}(t,x_H)\Big)\leq x_e(t)c_2(t).\end{aligned} \tag{66}$$

5.1 Output Feedback Design

Let y_r and $e=y-y_r$ be the reference power and reference tracking error, respectively. Define the output feedback

$$u(t)=\gamma e(t), \tag{67}$$

where $\gamma>0$. The error dynamics become

$$\dot{e}(t)=-\gamma c_1(t)e(t)+c_4(t)+\sigma c_3(t)-x_{\rm sp}c_2(t)-\dot{y}_r \tag{68}$$

which gives

$$\begin{aligned}\frac{\rm d}{{\rm d}t}|e|=&-\gamma c_1|e|+\Big(c_4+\sigma c_3-x_{\rm sp}c_2-\dot{y}_r\Big){\rm sign}(e)\\ \leq&-\gamma c_1|e|+|c_4+\sigma c_3-x_{\rm sp}c_2-\dot{y}_r|\\ \leq&-\gamma c_1|e|+|c_2||x_e-x_{\rm sp}+\sigma|+|\dot{y}_r|,\end{aligned} \tag{69}$$

where $|e(t)|$ is the absolute value of the error.

Note that $c_1(t)$ indicates the accumulated absolute power variation on the switch boundaries and it is positive and bounded under normal working conditions

$$L_1\leq c_1(t)\leq U_1, \tag{70}$$

where L_1 and U_1 are positive finite numbers. Given $RC\geq L_\tau>0$, we can show that $c_2(t)$ is bounded

$$0<|c_2(t)|\leq\frac{U_1}{L_\tau}. \tag{71}$$

We assume

$$|x_e-x_{\rm sp}+\sigma|\leq U_x \tag{72}$$

$$|\dot{y}_r|\leq U_y, \tag{73}$$

where U_x, and U_y are finite positive numbers. Using (70)–(73) we rewrite (69) as follows

$$\frac{\rm d}{{\rm d}t}|e|\leq-\gamma L_1|e|+\frac{U_1U_x}{L_\tau}+U_y, \tag{74}$$

and by applying the comparison principle [17] we get

$$|e(t)|\leq|e(0)|\exp(-\gamma L_1t)+\left(\frac{U_1U_x}{L_1L_\tau}+\frac{U_y}{L_1}\right)\frac{1}{\gamma}. \tag{75}$$

Note that $U_1U_x/(L_1L_\tau)+U_y/L_1$ is of the order of $O(1)$ and (75) is simplified as

$$|e(t)|\leq|e(0)|\exp\Big(-\gamma L_1t\Big)+O\left(\frac{1}{\gamma}\right). \tag{76}$$

If the feedback gain, $\gamma>0$, is large enough, then the error settles down to a small neighborhood around zero and reference tracking is achieved. The inverse of γ defines the neighborhood width. Higher feedback gains reduce the steady state error. However, a large feedback gain may drive the set-point temperature outside the working region of $[x_{\min},x_{\max}]$, particularly in response to large step changes in the reference power. Also, large feedback gains create chattering around the reference power during steady state. Hence, we suggest the reader to select the feedback gain moderately with respect to the reference power and environmental temperature variation.

5.2 State Feedback Design

The proposed control of (67) sacrifices tracking precision in favor of the implementation and design simplicity of output feedback. One may alternatively use a state feedback control to achieve perfect reference tracking. Denote a Lyapunov function as

$$V(t)=\frac{1}{2}e^2(t). \tag{77}$$

Define the following state feedback rule

$$u(t)=\gamma e(t)-\frac{c_2(t)x_{\rm sp}-c_3(t)\sigma-c_4(t)+\dot{y}_r}{c_1(t)}, \tag{78}$$

where $c_i(t)$ for $i=1,2,3,4$ require state measurements according to (63)–(66). Particularly, the population of units inside the

deadband which are changing state from on to off or vice versa need to be measured. Due to continuous evolution of the units between on and off state, temperature monitoring and measurement of all the TCL units regardless of their temperature level is required to implement the state feedback.

Take the time derivative of the Lyapunov function

$$\begin{aligned}\dot{V}(t) &= \dot{e}(t)e(t) \\ &= -\gamma c_1(t)e^2(t) \leq 0,\end{aligned} \tag{79}$$

which proves that the error uniformly asymptotically goes to zero.

Using (63)–(66) we can show that

$$\frac{c_2(t)x_{\text{sp}} - c_3(t)\sigma - c_4(t) + \dot{y}_r}{c_1(t)} \leq \frac{U_x}{L_\tau} + \frac{U_y}{L_1} \ll \gamma|e(t)|, \tag{80}$$

which predicts (67) is a good estimate of the state space control feedback of (78). Moreover, the closed-loop performance improvement and difficulties attached with implementing a state feedback control, which requires a considerable amount of temperature measurement, may not justify the idea of a state feedback control.

As shown in Section 3, the system dynamics (9) in combination with (12), (13), (16), and (17) are stable for every $x_{\text{sp}} \in [x_{\min}, x_{\max}]$.

We summarize the results of the power control design in the following theorem.

Theorem 1. *Consider an HrTCL population modeled by transport PDEs* (9)*, coupled through the boundary conditions* (12)*,* (13)*,* (16)*, and* (17) *with power consumption defined as* (19)*. Assume the accumulated absolute power variation at x_L and x_H is bounded by* (70) *and environmental temperature, x_e, and the reference power, y_r, satisfy* (72) *and* (73)*, respectively. Also, the time constant of TCLs satisfies $RC \geq L_\tau > 0$. Then, the output feedback control of* (67) *with $\gamma > 0$ governs the power consumption to an $O(1/\gamma)$-neighborhood of y_r. A state feedback control law as defined by* (78) *results in uniform asymptotic stability of the error dynamics.*

6 Simulation Results

According to our discussion in Section 5 about output and state feedback design and their differences, we continue our work with the output feedback control (67). We present simulation results to show the effectiveness of our proposed modeling and output feedback algorithm using the model and parameters presented in Section 4 with $\gamma = 0.01$. We assume, at the initial

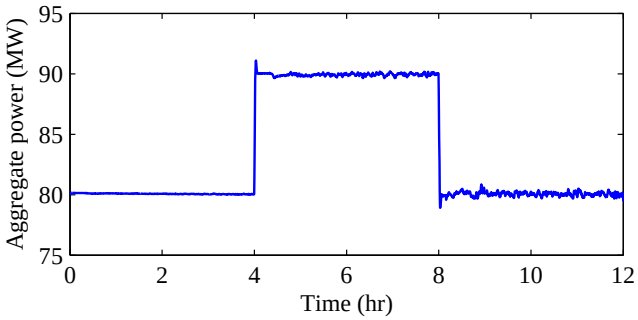

Figure 11. Reference tracking for step changes in power level.

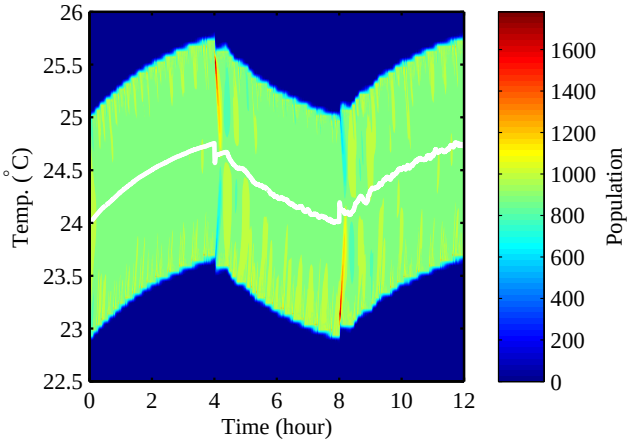

Figure 12. Spatial distribution of TCL units remains practiaclly uniform in the deadband. White line shows set-point evolution.

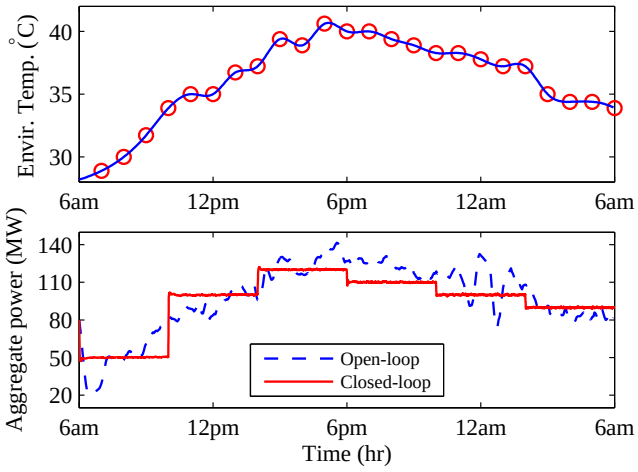

Figure 13. (above) Hourly variation of environmental temperature in Phoenix, Arizona, from July 13th 6:00 AM until July 14th 6:00 AM, 2013 [18]. (below) Variation of power versus time for (dashed blue) open-loop and (solid red) closed-loop system. The customer designs the power steps according to his/her priorities.

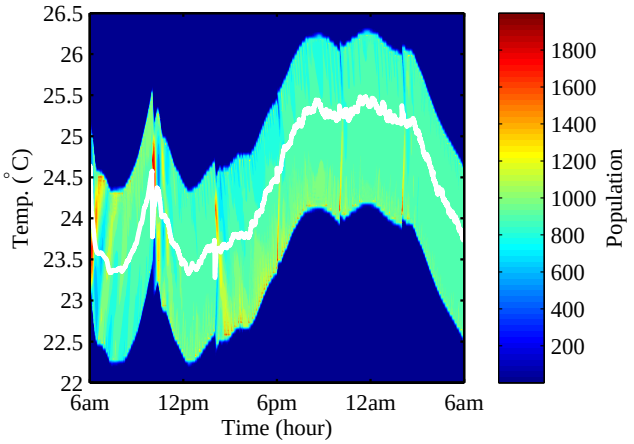

Figure 14. Evolution of the deadband and TCL population versus time. White line shows set-point evolution.

point, all units are located inside the deadband and evenly distributed between on and off states. We use the MC model to certify the credibility of the proposed control algorithm.

We present 3 different scenarios in this section: i) Output tracking for step changes in the reference power, ii) Power shaping under daily temperature variation, and iii) Power outage and transient analysis.

Reference tracking performance is shown in Fig. 11 for step changes in power at time $t = 4$ hr from 80 MW to 90 MW and then back to 80 MW at $t = 8$ hr. Deadband adaptation over time is shown in Fig. 12. Due to slow response time of the system and initial distribution of the TCL units, set-point temperature varies slowly. The proposed control algorithm updates the set-point temperature slightly at each time step to maintain the power at a fixed level.

Next we apply a daily environmental temperature curve, as shown in the top part of Fig. 13 for Phoenix, Arizona, from July 13th 6:00 AM until July 14th 6:00 AM, 2013 [18], to evaluate the performance of our power control technique. We present the response of our proposed control compared to the open-loop scenario in the bottom part of Fig. 13. The controller successively maintains the system at the user defined power levels. Adaptation process of the deadband and TCL population is shown in Fig. 14. We do not intend to design power shaping algorithms here. The proposed power steps are designed intuitively. Nevertheless, the user can design more sophisticated reference power steps using predictive control algorithms to mitigate both peak power and rate payer discomfort.

Natural and or man-made disasters could halt power flow. The peak power after power restoration could potentially put the system at risk. As shown in Fig. 15, a half an hour power outage, from $t = 1$ hr to $t = 1.5$ hr, causes all the TCL units to turn on with a slight delay which forces high power demand on the

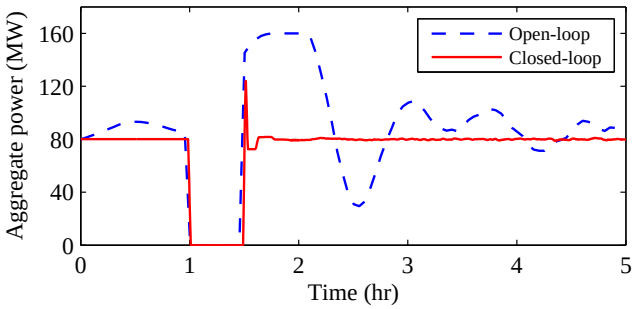

Figure 15. Power outage happens from $t = 1$ hr to $t = 1.5$ hr. Power consumption for (dashed blue) open-loop and (solid red) closed-loop system.

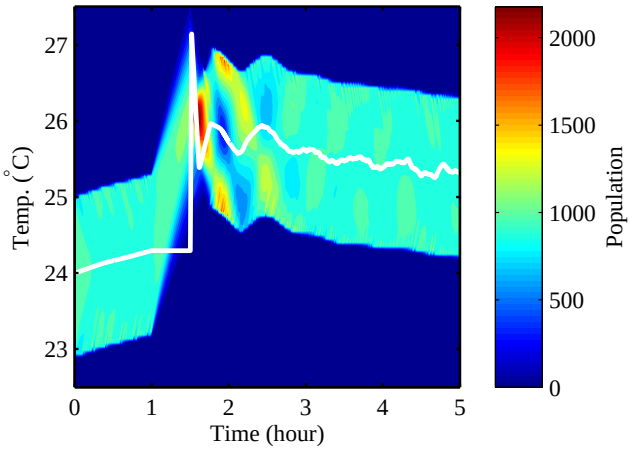

Figure 16. Evolution of the deadband and TCL population during power control. White line shows set-point evolution.

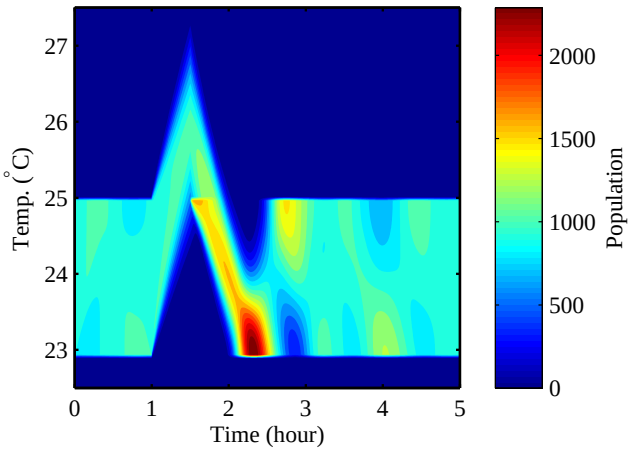

Figure 17. Static deadband and TCL population without power control. A large TCL population is turning on as power is restored.

power network. This is due to TCL heating beyond x_H. Moreover, the delay location, if matched with the peak demand, creates even more challenges with issues regarding the stability of the power network. Our proposed control dramatically reduces the peak power and governs the system to the reference power by slightly changing the set-point temperature as shown in Fig. 16. As shown in Fig. 17, without the power control the deadband remains static and TCL population experiences high density for on units right after power is restored. This causes high peak power during transient and low frequency oscillation in steady state power demand.

7 Conclusions

We model heterogeneous populations of thermostatically controlled loaded (TCLs) using parametrized transport partial differential equations (PDEs) coupled on the switch deadband boundaries. This work presents an analytically derived state-space model of heterogenous TCL (HrTCL) populations. The proposed model facilitates the precise simulation of various real-life scenarios in heating, cooling, and air conditioning (HVAC) systems. The model uses parametrization to consider the effect of heterogeneity in the physical characteristics of the TCL system. We investigate model stability, apply the finite difference method, and present guidelines to guarantee the numerical stability of the discretized dynamics. As shown in the reported simulations, the model effectively predicts system performance under daily variation of environmental temperature and power outage enforced by load management programs. Moreover, we have shown that the reference power tracking problem for the HrTCL system can be solved using a linear integrator with a proper gain. The simulation results demonstrate the effectiveness of the proposed control algorithm.

REFERENCES

[1] Bashash, S., and Fathy, H. K., 2013. "Modeling and control of aggregate air conditioning loads for robust renewable power management". *IEEE Transactions on Control Systems Technology,* **21**, pp. 1318 – 1327.

[2] Moura, S., Ruiz, V., and Bendtsen, J., 2013. "Modeling heterogeneous populations of thermostatically controlled loads using diffusion-advection PDEs". In Proc. of ASME Dynamic Systems and Control Conference.

[3] Moura, S., Bendtsen, J., and Ruiz, V., 2013. "Observer design for boundary coupled PDEs: application to thermostatically controlled loads in smart grids". In Proc. of IEEE Conference on Decision and Control.

[4] Zhang, W., J. Lian, C.-Y. C., and Kalsi, K., 2013. "Aggregated modeling and control of air conditioning loads for demand response". *IEEE Transactions on Power Systems,* **28**, pp. 4655 – 4664.

[5] Lu, N., and Chassin, D. P., 2004. "A state-queueing model of thermostatically controlled appliances". *IEEE Transactions on Power Systems,* **19**, pp. 1666–1673.

[6] Chassin, D. P., and Fuller, J. C., 2011. "On the equilibrium dynamics of demand response in thermostatic loads". In Proc. of 44th Hawaiian International Conference on System Sciences.

[7] Kalsi, K., Chassin, F., and Chassin, D., 2011. "Aggregate modeling of thermostatic loads in demand response: a systems and control perspective". In Proc. of IEEE Conference on Decision and Control and European Control Conference.

[8] Callaway, D. S., 2009. "Tapping the energy storage potential in electric loads to deliver load following and regulation, with application to wind energy". *Energy Conversion and Management,* **50**, pp. 1389–1400.

[9] Soudjani, S. E. Z., and Abate, A., 2013. "Aggregation of thermostatically controlled loads by formal abstractions". In Proc. of European Control Conference.

[10] Koch, S., Mathieu, J. L., and Callaway, D. S., 2011. "Modeling and control of aggregated heterogeneous thermostatically controlled loads for ancillary services". In Proc. of 17th Power Systems Computation Conference.

[11] Mortensen, R. E., and Haggerty, K. P., 1990. "Dynamics of heating and cooling loads: models, simulation, and actual utility data". *IEEE Transactions on Power Systems,* **5**, pp. 243–249.

[12] Malhame, R., and Chong, C.-Y., 1985. "Electrical load model synthesis by diffusion approximation of a high-order hybrid-state stochastic system". *IEEE Transactions on Automatic Control,* **AC-30**, pp. 854–860.

[13] Ihara, S., and Schweppe, F. C., 1981. "Physically based modeling of cold load pickup". *IEEE Transactions on Power Apparatus and Systems,* **PAS-100**, pp. 4142–4150.

[14] Chong, C. Y., and Debs, A. S., 1979. "Statistical synthesis of power system functional load models". In Proc. of IEEE Conference on Decision and Control.

[15] Sanandaji, B. M., Hao, H., and Poolla, K., 2014. "Fast regulation service provision via aggregation of thermostatically controlled loads". In Proc. of 47th Hawaii International Conference on System Sciences.

[16] Hao, H., Sanandaji, B. M., Poolla, K., and Vincent, T. L., 2015. "Aggregate flexibility of thermostatically controlled loads". *IEEE Transactions on Power Systems,* **30**, pp. 189–198.

[17] Khalil, H. K., 1996. *Nonlinear Systems*, second ed. Prentice Hall, NJ: Englewood Cliffs.

[18] wunderground, 2013. "Weather history for Phoenix, AZ". In `http://www.wunderground.com/history/airport/KPHX/2013/7/13/DailyHistory.html`.